



Regional Moment Tensor Inversion using Rotational Observations

Gene A. Ichinose, Sean R. Ford and Robert J. Mellors

Lawrence Livermore National Laboratory

American Geophysical Union Fall Meeting, San Francisco, CA 9-13 December 2019. S032 - Rotation and Strain in Seismology - Applications, Instrumentation and Theory. Tuesday 10 Dec 2019 08:00-12:00 5216-0589

This work was performed under the auspices of the US Department of Energy by Lawrence Livermore National Laboratory under contract DE-AC52-07NA27344. Release #LLNL-POST-798406

Introduction / Summary

1. We use the simplest approach to calculate rotational Greens functions for incorporating into regional moment tensor (MT) inversions (see section 2).
2. We did not have three-component (3-C) rotational data "yet" so we used array-derived rotations from the Pinon Flat Observatory in California and Goley array in Enid, Oklahoma. We successfully demonstrate inclusion of 3-C rotational with 3-C translational data into MTINV version 4.0.0 [<https://sourceforge.net/projects/mtinv/>] (see section 3).
3. We examined the sensitivity of Full-MT solutions by including 3-C rotational data with regular translational displacement data using Network Sensitivity Solution (NSS) approach by plotting the percent variance reduction on Eigenvalue sphere or Lunc (see section 4).
4. The examples of two and three-station 3-C datasets with 3-C rotational data improved the MT solution sensitivity, by increasing Double-Couple (DC) components and reducing Compensated Linear Vector Dipole (CLVD) and isotropic (ISO) components relative to using just the 3-C translational displacement data alone (see section 4).

Motivation: Donner et al. (2016) published a paper titled, "Inversion for seismic moment tensors combining translational and rotational ground motions." Their encouraging study is based on synthetic scenarios and states: "Our results indicate that the resolution of the moment tensor can be increased drastically by incorporating rotational ground motion data. Especially, the usually problematic components M_{xz} and M_{yz} as well as all components containing spatial derivatives with depth..."

1. Exploring Rotational and Displacement Synthetics and Radiation Patterns using a Gradient 3-D Velocity Model

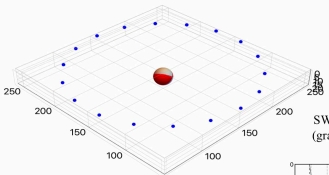
1.1) The displacement radiation patterns are provided by Aki and Richards (2002) Equation 4.33 and the far-field S is:

$$AFS = \cos(2\theta)\cos(\phi)\theta - \cos(\theta)\sin(2\phi)\phi$$

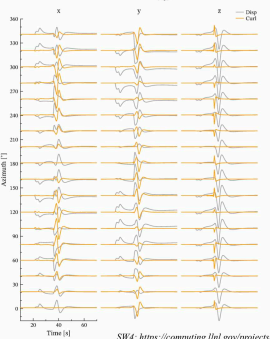
where θ and ϕ are the unit vectors in the spherical coordinate system (shown in Aki and Richards (2002) Figure 4.4). The rotation radiation pattern is provided by Cochard et al. (2006) Equation 30.4. The far-field rotation is a function of the derivative of the moment-rate function and its radiation pattern is:

$$AR = \cos(\theta)\sin(\phi)\theta - \cos(2\theta)\sin(\phi)\phi$$

1.3) Thus, one six-component (6-C) station can gather the same information on radiation pattern as two three-component (3-C) stations at 90° azimuth from one another along the focal plane axis, which is sometimes difficult to obtain when restricted to surface sensors. Additionally, information on the derivative of the moment-rate function can be obtained in the far-field, which would provide a constraint on the source-time function, though not in the case of long-period moment tensors, where the source-time function is taken as a step (or moment-rate delta). We demonstrate the difference in the waveform by simulating the displacements and rotations at a distance of 100 km from a M 5 normal faulting (strike = 23°, rake = -76°, dip = 50°) earthquake (Brune (1970) source displacement with 1-sec rise-time) at a depth of 10 km.



SW4 simulation comparison of displacement for the homogeneous (gray) and gradient (black) medium for the velocity profiles shown below. The gradient synthetics are shifted by 3-seconds.

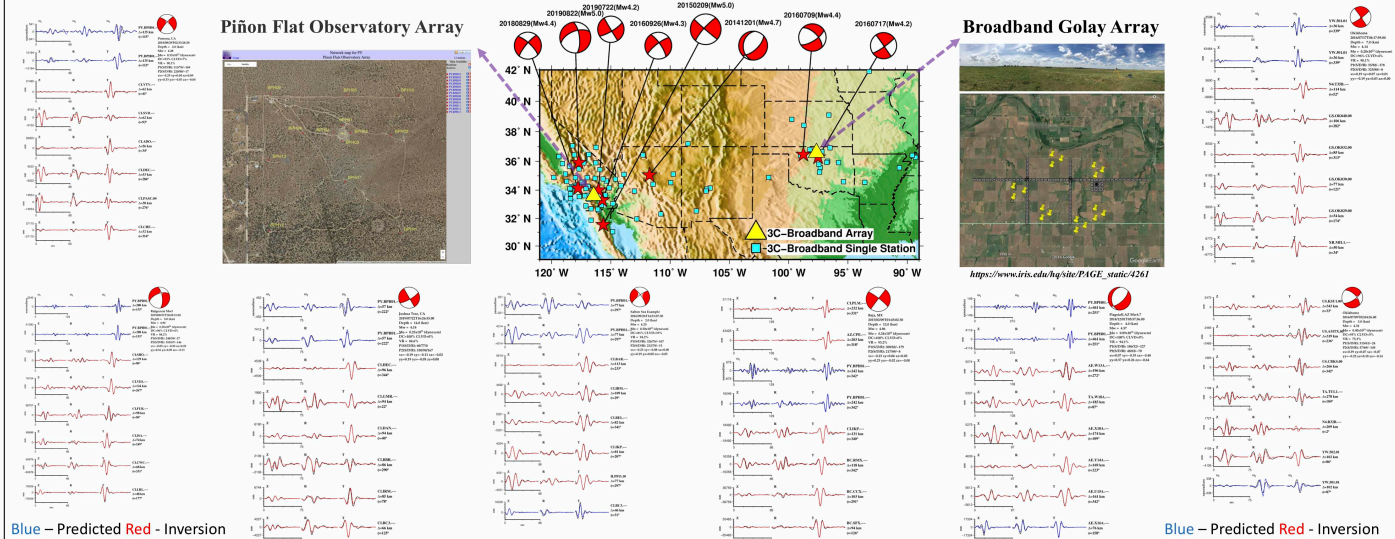


SW4 simulations of displacement (gray) and rotation (orange) for a constant velocity half-space ($v = 5000$ m/s, $\beta = 2900$ m/s and $\rho = 2650$ kg/m³). The rotation (curl) is multiplied by a factor of 1000.

SW4 simulation comparison of rotation for the homogeneous (orange) and gradient (red) medium for the velocity profiles shown above. The gradient synthetics are shifted by 3-seconds.

SW4: <https://computing.llnl.gov/projects/terpenite-wave-propagation>

3. Waveform Data and Deviatoric Moment Tensor Inversion Results: Broadband 3-C Arrays and 3-C Single Stations



2. Methods: Computing Rotational Green Functions for MT Inversion

- Rotational motions computed using 5-point stencil.
 - GFs are computed at 4 points around corner reference point (see right) for each fundamental faulting orientation (S, SW, NW) and isotropic GFs.
 - Spatial gradient computed using 2-point finite difference along the X- and Y-axes
 - Rotate 3-components from vertical, radial, transverse (L,R,T) to vertical, north, east (U,V,W) coordinates
- Associate the component of rotation to P-SV or SH radiation patterns (e.g., Benhoff & Gutenberg, 1952; Pascal & Mayvezet, 2013; Li & Baan, 2017)
 - $\omega = \text{rotation rate vector}$
 - $\beta = \text{slowness vector (z-radial, x-tangential, y-vertical)}$
 - is displacement
 - $\omega_x = \beta_y \cdot \partial_x u - \beta_x \cdot \partial_y u$
 - $\omega_y = -\beta_x \cdot \partial_x u - \beta_y \cdot \partial_y u$
 - The rotation about the x and y axes should scale with vertical component and therefore have a P-SH radiation pattern.
 - The rotation about the z axis scales with the tangential component and therefore has the SH-wave radiation pattern.

Free Surface Effects - strain and rotation
 Zero traction boundary condition at free surface implies that $\sigma_{11} = \sigma_{22} = \sigma_{33} = 0$ ($\sigma = \sigma_{ij} = \sigma_{ji}$). Hooke's law is $\sigma_{ij} = \lambda \delta_{ij} \epsilon_{kk} + 2\mu \epsilon_{ij}$ in homogeneous isotropic medium leads to:

$$\sigma_{11} = \lambda(\epsilon_{11} + \epsilon_{22} + \epsilon_{33}) + 2\mu\epsilon_{11} = 0$$

$$\sigma_{22} = \lambda(\epsilon_{11} + \epsilon_{22} + \epsilon_{33}) + 2\mu\epsilon_{22} = 0$$

$$\sigma_{33} = \lambda(\epsilon_{11} + \epsilon_{22} + \epsilon_{33}) + 2\mu\epsilon_{33} = 0$$

$$\epsilon_{11} = -\frac{2\mu}{\lambda + 2\mu}\epsilon_{22} = -\frac{2\mu}{\lambda + 2\mu}\epsilon_{33}$$

$$\epsilon_{22} = -\frac{2\mu}{\lambda + 2\mu}\epsilon_{11} = \frac{2\mu}{\lambda + 2\mu}\epsilon_{33}$$

$$\epsilon_{33} = \frac{\lambda + \mu}{\lambda + 2\mu}\epsilon_{11} = \frac{\lambda + \mu}{\lambda + 2\mu}\epsilon_{22}$$

This slide shows best comparisons between accelerations and scaled rotation rates

- Fundamental Faulting Orientations & Isotropic:
 - Vertical strike slip (SS)
 - 45 degree dip slip (DS)
 - Vertical dip slip (VDS)
 - Isotropic
- An effectively synthetic: Distance = 737 km, Depth = 6 km, Bandpass Filter (0.05-2.5 Hz)
- The ω_x rotations have a SH radiation pattern
- The ω_y and ω_z rotations have a P-SH radiation pattern
- is the rotation the far-field motion
- This allows for incorporation into the linear moment tensor inversion based on the SS, DS, VDS, ISO Green function formulation (i.e. synthetics are linear combination of GFs with ω_{ij})

Array-Derived Rotations (Spudich et al., 1995)

$$r^T = [r_1^T \ r_2^T \ \dots \ r_N^T]^T, \quad r_i = 0, 1, \dots, N$$

$$M^T = [M_1^T \ M_2^T \ \dots \ M_N^T]^T, \quad M_i = u^T \cdot u^i - u^i \cdot u^T$$

$$G = \begin{pmatrix} G_{11} & G_{12} & G_{13} \\ G_{21} & G_{22} & G_{23} \\ G_{31} & G_{32} & G_{33} \end{pmatrix}, \quad G_{ij} = M_{ij}^T \cdot M_j$$

Moment Tensor Formulation

$$M_{11} = M_{11}^{SS} \frac{2Z(2\alpha_1) - Z(0)}{2} + M_{11}^{DS} \frac{2Z(\alpha_1) - Z(0)}{3} + M_{11}^{VDS} \frac{2Z(\alpha_1) - Z(0)}{3} + M_{11}^{ISO} \frac{2Z(\alpha_1) - Z(0)}{3}$$

$$M_{22} = M_{22}^{SS} \frac{2Z(2\alpha_2) - Z(0)}{2} + M_{22}^{DS} \frac{2Z(\alpha_2) - Z(0)}{3} + M_{22}^{VDS} \frac{2Z(\alpha_2) - Z(0)}{3} + M_{22}^{ISO} \frac{2Z(\alpha_2) - Z(0)}{3}$$

$$M_{33} = M_{33}^{SS} \frac{2Z(2\alpha_3) - Z(0)}{2} + M_{33}^{DS} \frac{2Z(\alpha_3) - Z(0)}{3} + M_{33}^{VDS} \frac{2Z(\alpha_3) - Z(0)}{3} + M_{33}^{ISO} \frac{2Z(\alpha_3) - Z(0)}{3}$$

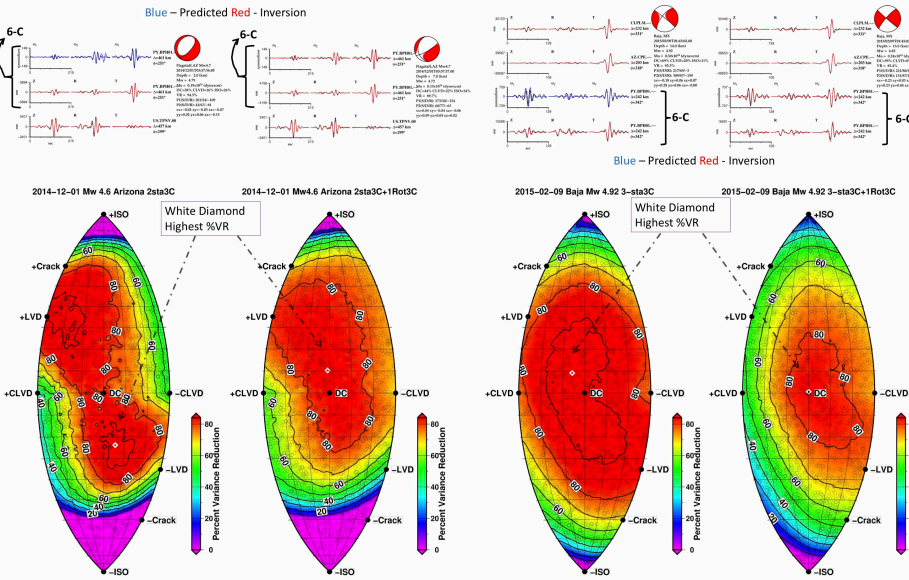
$$M_{12} = M_{12}^{SS} \frac{2Z(\alpha_1) - Z(0)}{3} + M_{12}^{DS} \frac{2Z(\alpha_1) - Z(0)}{3} + M_{12}^{VDS} \frac{2Z(\alpha_1) - Z(0)}{3} + M_{12}^{ISO} \frac{2Z(\alpha_1) - Z(0)}{3}$$

$$M_{13} = M_{13}^{SS} \frac{2Z(\alpha_1) - Z(0)}{3} + M_{13}^{DS} \frac{2Z(\alpha_1) - Z(0)}{3} + M_{13}^{VDS} \frac{2Z(\alpha_1) - Z(0)}{3} + M_{13}^{ISO} \frac{2Z(\alpha_1) - Z(0)}{3}$$

$$M_{23} = M_{23}^{SS} \frac{2Z(\alpha_2) - Z(0)}{3} + M_{23}^{DS} \frac{2Z(\alpha_2) - Z(0)}{3} + M_{23}^{VDS} \frac{2Z(\alpha_2) - Z(0)}{3} + M_{23}^{ISO} \frac{2Z(\alpha_2) - Z(0)}{3}$$

4. Full Moment Tensor Inversion Sensitivity Results (Network Sensitivity Solutions) with and without Rotational 3-C Data

We performed MT inversions on 2- and 3-station datasets. The station referred to as the 6-C is the array with the 3-C rotation plus 3-C reference site displacement. All the single 3-C stations selected were about the same distance as the 3-C arrays. The 3-C rotational data were weighted by a factor of approx. 40 so they were the same amplitude range as the 3-C translational displacements.



- Signs of MT solution improvement with rotational data:
1. Point of highest %VR moves closer to the origin (or highest %DC).
 2. The 80% VR contour decreases in size and covers the origin.
 3. The 80% VR contour centered on origin rather than bi-modal distribution